


 Cite this: *RSC Adv.*, 2024, 14, 39636

TiO₂/CuWO₄ heterojunction photocatalyst in the preparation of cardiovascular chromeno[4,3-*b*]chromene drugs†

 Jiaqi Sun and Jiahao Song *

Chromeno[4,3-*b*]chromenes have shown potential as effective drugs against cardiovascular diseases. This study centered on a novel heterojunction nanocomposite TiO₂/CuWO₄, which incorporates titanium dioxide (TiO₂) and copper tungstate(vi) to improve photocatalytic efficiency. The characterization of the TiO₂/CuWO₄ photocatalyst was performed using various techniques, including FT-IR, XRD, TEM, DRS, SEM, EDS, and XPS. TiO₂/CuWO₄ demonstrated significant effectiveness as a photocatalyst for the synthesis of chromeno[4,3-*b*]chromene derivatives, which show potential antibacterial and antifungal properties beneficial for oral health concerns such as dental caries and periodontal disease. While TiO₂ can absorb light to produce electrons and holes under direct illumination, its photocatalytic efficiency is improved when paired with CuWO₄. The research also explored the influence of several factors, including the quantity of photocatalyst, reaction duration, temperature, solvent selection, and the reusability of the nanocomposite. Optimal reaction conditions were found to involve 1 mmol of dimedone, benzaldehyde, and 4-hydroxycoumarin, using 12 mg of TiO₂/CuWO₄ in 4 mL of ethanol, subjected to irradiation from a green laser at room temperature for 30 minutes. The results indicate that the TiO₂/CuWO₄ heterojunction ranks among the most effective options for photocatalytic synthesis of chromeno[4,3-*b*]chromene derivatives.

 Received 4th November 2024
 Accepted 3rd December 2024

DOI: 10.1039/d4ra07857h

rsc.li/rsc-advances

1. Introduction

Chromeno[4,3-*b*]chromenes are a class of compounds that have garnered attention for their potential therapeutic effects, including activities against cardiovascular diseases. These compounds have shown antihypertensive effects, which could be beneficial in managing cardiovascular diseases. Moreover, chromenes are noted for their antioxidative capabilities, and can play a crucial role in cardiovascular health by reducing oxidative stress, atherosclerosis and hypertension.^{1–3} Chromeno[4,3-*b*]chromenes may exhibit anti-inflammatory effects that could mitigate the inflammatory processes associated with diseases like coronary artery disease and heart failure. Therefore, the synthesis of chromeno[4,3-*b*]chromenes is significant in drug design due to their diverse biological activities and structural versatility, making them valuable scaffolds for developing new therapeutic agents. The ability to synthesize chromeno[4,3-*b*]chromenes through various efficient methodologies enhances their accessibility for drug development.

Heterojunction photocatalysis has attracted considerable attention from researchers in recent years for several important

reasons. A main issue with conventional semiconductor photocatalysts is the swift recombination of photogenerated electron–hole pairs, which reduces their efficiency.^{4–7} Heterojunction systems effectively enhance the separation and movement of these charge carriers, resulting in improved photocatalytic performance. By combining various semiconductors, we can develop structures that promote more efficient charge transfer and minimize recombination rates.⁸ Additionally, heterojunctions can be tailored to capture a broader spectrum of solar energy, particularly in the visible range, which is essential for effective applications in environmental cleanup and energy conversion.^{9–13} TiO₂/CuWO₄ heterojunction is an efficient photocatalyst due to its unique structural and electronic properties. The effectiveness of TiO₂/CuWO₄ as a photocatalyst primarily stems from its ability to facilitate the separation of photogenerated charge carriers. The unique band alignment between TiO₂ and CuWO₄ allows for efficient transfer of these charges, minimizing recombination rates. CuWO₄ can accept electrons from TiO₂ due to its more positive conduction band edge potential, which enhances the overall photocatalytic efficiency by extending the lifetime of the charge carriers.

In this research, the synthesis of chromeno[4,3-*b*]chromenes was selected as a model for a multi-component reaction.^{14,15} The cyclocondensation process used to generate these compounds is a significant transformation in organic synthesis, yielding well to excellent results. This study thoroughly examines the

Department of Cardiology, The Second Affiliated Hospital of Xinjiang Medical University, Urumqi City, 830000, China. E-mail: songjiahaourumqi@outlook.com

† Electronic supplementary information (ESI) available. See DOI: <https://doi.org/10.1039/d4ra07857h>



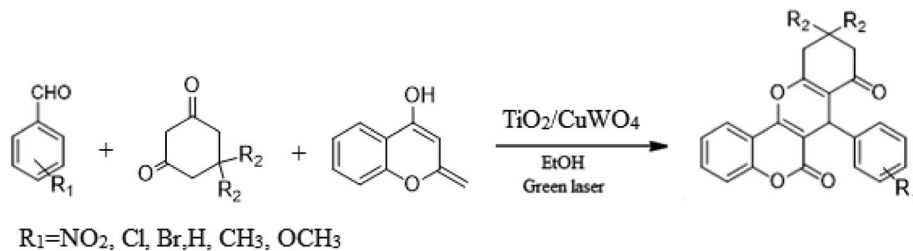


Fig. 1 Production of various substituted chromeno[4,3b]chromenes.

influence of various factors, such as the quantity of photocatalyst, reaction duration, temperature, and solvent choice, along with the reusability of the nanocomposite. The addition of CuWO_4 to TiO_2 alters the overall efficiency of the photocatalyst and improves its performance. The enhanced quality of the final $\text{TiO}_2/\text{CuWO}_4$ is attributed to the fact that TiO_2 mainly absorbs UV light, which restricts its effectiveness under visible light. In contrast, CuWO_4 broadens the light absorption into the visible spectrum, facilitating improved photocatalytic activity. Additionally, the carried out modification can increase the production of reactive oxygen species, including hydroxyl radicals and superoxide anions. Thus, the integration of TiO_2 and CuWO_4 may lead to synergistic effects that enhance reaction pathways beyond what either component could accomplish independently. This study highlights the potential of $\text{TiO}_2/\text{CuWO}_4$ as a reusable catalyst for the efficient and sustainable synthesis of chromeno[4,3-*b*]chromene derivatives (Fig. 1).

2. Experimental

2.1 Materials and methods

Titanium isopropoxide ($\text{C}_{12}\text{H}_{28}\text{O}_4\text{Ti}$) was obtained from commercial suppliers, along with potassium and sodium hydroxides, copper(II) nitrate ($\text{Cu}(\text{NO}_3)_2 \cdot 6\text{H}_2\text{O}$), sodium tungstate dihydrate ($\text{Na}_2\text{WO}_4 \cdot 2\text{H}_2\text{O}$), and several organic compounds. The morphology of the photocatalyst was assessed using FE-SEM Mira 3-XMU. FT-IR spectra were collected using a PerkinElmer spectrophotometer, spanning the range of 400–4000 cm^{-1} . UV-Vis spectra were obtained with a Spekol 2000 UV-visible spectrophotometer. Powder X-ray diffraction (XRD) analysis was conducted using an Xpert MPD diffractometer, employing Cu $K\alpha$ radiation at 30 mA and 40 keV, with scans ranging from 5° to 80° at a speed of 3° per minute. The optical characteristics of $\text{TiO}_2/\text{CuWO}_4$ were analyzed using diffuse reflectance spectroscopy (DRS) conducted with a Shimadzu UV-2450 spectrophotometer across a wavelength range of 80–200 nm. For transmission electron microscopy (TEM) analysis, a PHILIPS TECNAI 10 microscope was employed, complemented by energy dispersive X-ray spectroscopy (EDS). X-ray photoelectron spectroscopy (XPS) was also conducted using a Thermo Fischer Scientific ESCALAB instrument.

2.2 Synthesis of titanium dioxide (TiO_2)

To prepare titanium oxide nanoparticles, a 30 mL solution of 0.1 M titanium isopropoxide was placed in a cold water bath,

kept at around 5 °C. Gradual addition of 5.0 M KOH was performed until the pH reached 7.0. After stirring the mixture for roughly 15 minutes, a white colloidal solid was formed. The volume of final solution was brought to 60 mL by adding distilled water. This mixture was then placed in a 120 mL Teflon autoclave and heated to 270 °C for 12 hours. The resulting precipitate was dried at 400 °C for 2 hours, yielding TiO_2 particles.^{16,17}

2.3 Synthesis of titanium dioxide/copper(II) tungstate ($\text{TiO}_2/\text{CuWO}_4$)

Initially, 15 mL of 1 M copper(II) nitrate was mixed with 1.5 mL of 0.5 M sodium tungstate dihydrate. After that, 0.25 g of titanium dioxide was added to this solution and stirred magnetically for 1.5 hours. The mixture was then sonicated for 25 minutes. Following this step, 25 mL of 4 M sodium hydroxide was added slowly to the mixture. Finally, the resulting solid was dried in an oven at 115 °C and calcined at 350 °C for 4 hours.^{18,19}

2.4 Synthesis of chromeno[4,3b]chromenes

For the synthesis of chromeno[4,3-*b*]chromenes, a test tube was prepared with 140 mg (1 mmol) of dimedone, 162 mg (1 mmol) of 4-hydroxycoumarin, and 100 mg (1 mmol) of benzaldehyde. To this mixture, 0.012 g of $\text{TiO}_2/\text{CuWO}_4$ was added as the catalyst. The mixture was then subjected to irradiation from a commercial green-light laser for 30 minutes at room temperature. The progress of the reaction was assessed using thin-layer chromatography (TLC). After the reaction was complete, 8 mL of water and 4 mL of ethyl acetate were introduced to the mixture to dissolve the product. The ethyl acetate layer was then separated, and the aqueous layer was extracted three times with EtOAc. The combined organic layer was then dried using sodium sulfate, and the final product was purified through column chromatography.^{20,21}

3. Results and discussion

3.1 Characterization of $\text{TiO}_2/\text{CuWO}_4$

3.1.1 Morphology studies. Utilizing FE-SEM and TEM techniques for the morphology studies of $\text{TiO}_2/\text{CuWO}_4$ plays a crucial role in revealing important information regarding size distribution, surface characteristics, and structural properties.²² The FE-SEM images (Fig. 2a and b) show that the morphology of the $\text{TiO}_2/\text{CuWO}_4$ particles is generally acceptable, although

signs of aggregation are noticeable. These images provide valuable insights into the overall structure and the degree of aggregation among the nanoparticles. A more detailed examination using TEM (Fig. 2c) was conducted to obtain refined information about the size and microstructure of the $\text{TiO}_2/\text{CuWO}_4$ nanoparticles. The TEM analysis revealed that particle size of the $\text{TiO}_2/\text{CuWO}_4$ particles ranges from approximately 50 to 250 nm, providing critical insights into the nanoscale dimensions of this material.

3.1.2 EDX. In addition, EDX mapping of the photocatalyst revealed information about the elemental distribution in $\text{TiO}_2/\text{CuWO}_4$. As shown in Fig. 3, the elements copper (Cu), titanium (Ti), oxygen (O), and tungsten (W) were detected in the photocatalyst. The atomic percentages of these elements are specified in the inset of Fig. 3.

3.1.3 FT-IR. FT-IR analysis offers valuable insights into the surface characteristics and chemical makeup of the $\text{TiO}_2/\text{CuWO}_4$ photocatalyst (Fig. 4). This technique aids in identifying the functional groups in $\text{TiO}_2/\text{CuWO}_4$. In the FT-IR spectrum of CuWO_4 , the bands observed at 970 and 756 cm^{-1} are attributed to the stretching vibrations of W–O and Cu–O bonds, respectively. The peak at 1627 cm^{-1} is associated with the carbonyl group from the titanium carboxylate, which is derived from the titanium isopropoxide precursor. Additionally, the weaker peaks at 805 cm^{-1} and 630 cm^{-1} correspond to Ti–O–C and Ti–O bonds, respectively. Consequently, peaks for TiO_2 and CuWO_4 were detected in $\text{TiO}_2/\text{CuWO}_4$.²³

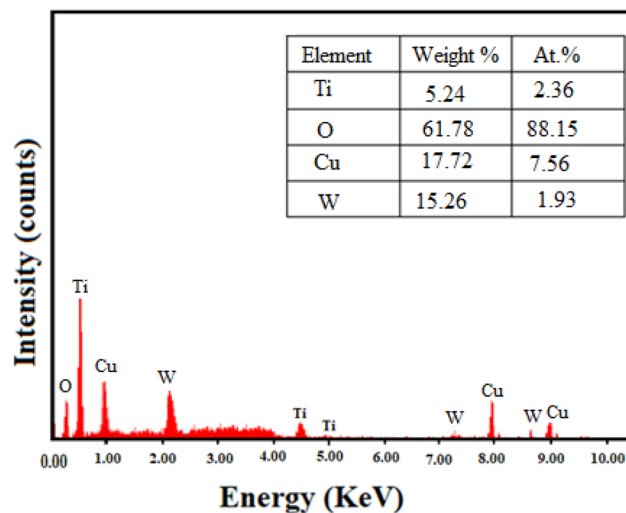


Fig. 3 EDX pattern of $\text{TiO}_2/\text{CuWO}_4$.

3.1.4 XRD. The XRD pattern shows peaks at the 2θ values of 18.1° , 25.9° , 26.1° , 36.9° , and 55.1° , which are associated with the crystalline planes (020), (111), (101), (004), and (105), respectively (Fig. 5). Additionally, the peaks at 17.2° and 34.1° correspond to the (020) and (002) planes of monoclinic tungsten trioxide. Meanwhile, the peaks at 26.1° , 36.9° , and 48.8° are linked to the (101), (004), and (200) crystal planes, indicating the

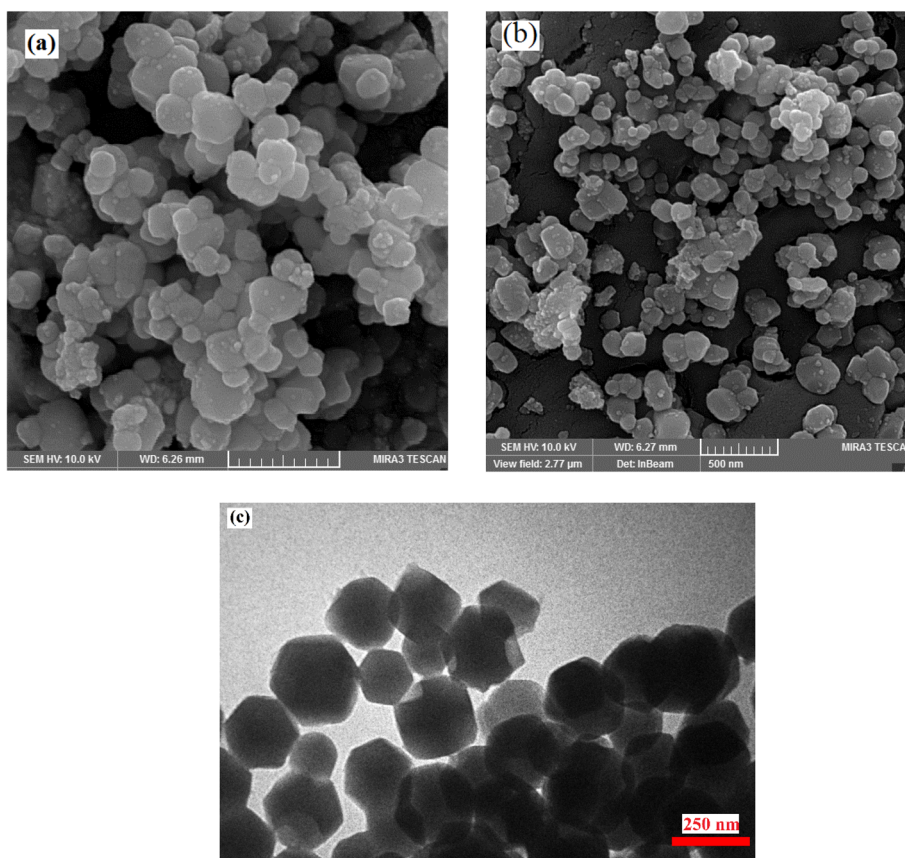


Fig. 2 FE-SEM images of (a) TiO_2 and (b) $\text{TiO}_2/\text{CuWO}_4$. (c) TEM image of $\text{TiO}_2/\text{CuWO}_4$.

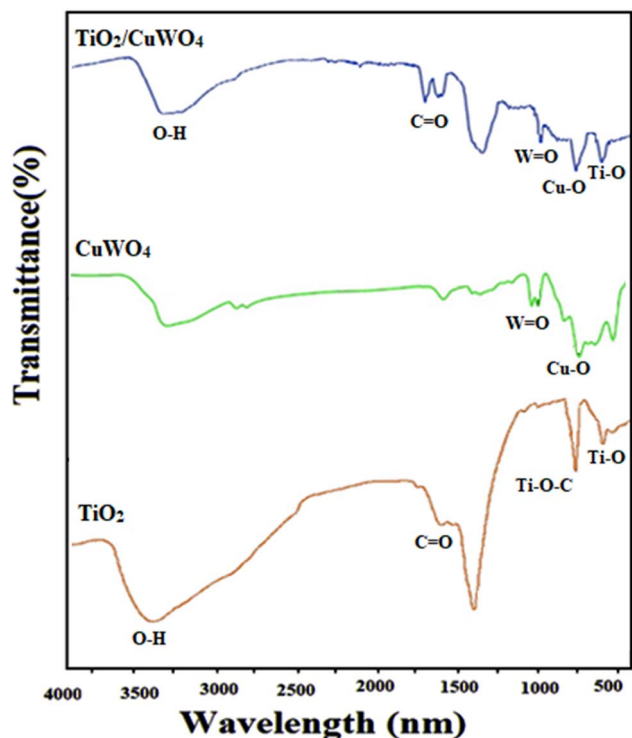


Fig. 4 FT-IR of $\text{TiO}_2/\text{CuWO}_4$, CuWO_4 , and TiO_2 .

presence of anatase form of TiO_2 . Conversely, peaks at 18.1° , 25.9° , 34.5° , 35.1° , 49.3° , and 52.3° correspond to the (020), (111), (111), (002), (202), and (222) planes of monoclinic tungsten trioxide.²⁴ Furthermore, weak peaks observed at 18.1° , 24.6° , 33.1° , 36.1° , 38.2° , and 42.1° are associated with the Miller indices (020), (021), (002), (111), (130), and (131) for CuO , indicating its incorporation in the $\text{TiO}_2/\text{CuWO}_4$ composite.

3.1.5 UV-Vis. Fig. 6a displays the UV-Vis spectrum of $\text{TiO}_2/\text{CuWO}_4$. The optical band gaps for TiO_2 (Fig. 6b), CuWO_4 (Fig. 6c), and $\text{TiO}_2/\text{CuWO}_4$ (Fig. 6d) were evaluated through Tauc analysis. TiO_2 has a wide band gap of about 3.2 eV, which suggests a tendency for the rapid recombination of the charge carriers generated by light, thus limiting its practical use. To assess the optical band gap of $\text{TiO}_2/\text{CuWO}_4$ in comparison to TiO_2 and CuWO_4 , the emission reflectance spectrum was recorded.

3.1.6 XPS. X-ray photoelectron spectroscopy (XPS) is a key method for examining the surface characteristics of $\text{TiO}_2/\text{CuWO}_4$ and can provide the chemical states and relative amounts of Ti 2p, W 4f, Cu 2p, C 1s, and O 1s (Fig. S1a–f†). The binding energies for Ti $2p_{3/2}$ and Ti $2p_{1/2}$, measured at 459.4 eV and 465.1 eV in Fig. S1b,† affirm the presence of titanium within the nanocomposite. The high-resolution spectra for Cu 2p reveal peaks at 934.31 eV and 954.15 eV, which correspond to Cu $2p_{3/2}$ and Cu $2p_{1/2}$, respectively. The difference in binding energy among these peaks suggests the presence of metallic copper, which confirms its existence in the sample shown in Fig. S1c.† In the W 4f region illustrated in Fig. S1d,† the binding energies for W $4f_{7/2}$ and W $4f_{5/2}$ are located at approximately 34.1 eV and 36.3 eV, respectively. These values align closely with

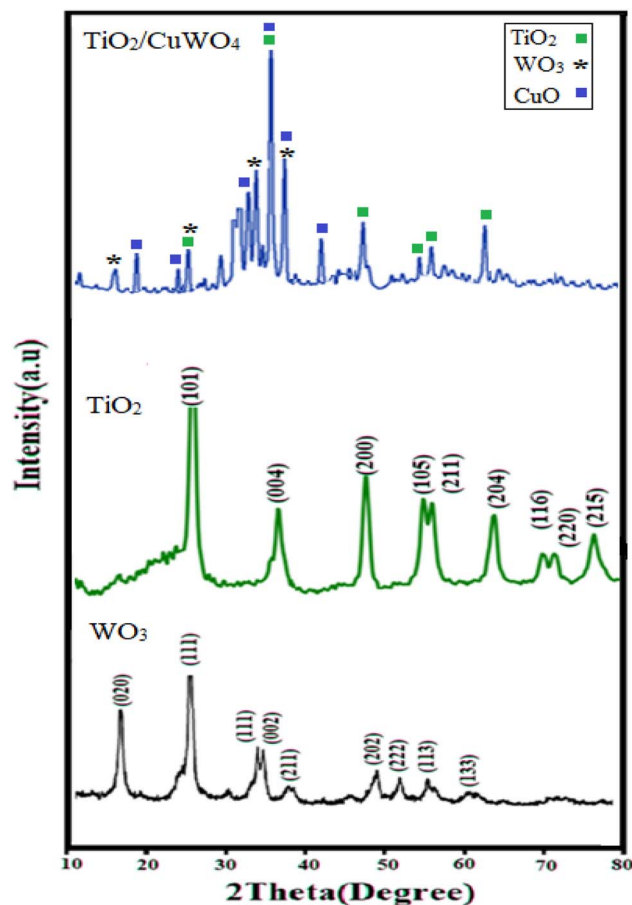


Fig. 5 XRD of $\text{TiO}_2/\text{CuWO}_4$.

the binding energies commonly associated with WO_3 , providing further evidence of its presence in the material. Fig. S1e† shows the high-resolution XPS spectra for O 1s, where a binding energy peak at 531.32 eV is attributed to oxygen atoms in Ti–O and W–O bonds, suggesting shared orbital characteristics between these species. In Fig. S1f,† the XPS spectrum for C 1s reveals three distinct peaks at 284.9 eV, 286.1 eV, and 288.5 eV, corresponding to C–C bonds, C–O, and O=C–O groups, respectively.²⁵

3.2 Catalytic tests

3.2.1 Photocatalyst amount, reaction time, temperature, and solvent effects. The standard reaction was performed without a photocatalyst and with different amounts of $\text{TiO}_2/\text{CuWO}_4$ to find the ideal quantity for the best results. The optimal efficiency was observed with 0.012 g of the photocatalyst (Fig. 7). To identify the best reaction time, experiments were carried out for varying lengths, with peak efficiency reached at the 30 minutes. The findings showed that increasing the reaction time beyond 30 minutes did not lead to a meaningful improvement in efficiency (Fig. 8). Furthermore, several photocatalysts were tested under standard conditions to find the most effective catalyst for photocatalytic activity (all 0.012 g). This study concluded that the $\text{TiO}_2/\text{CuWO}_4$ photocatalyst

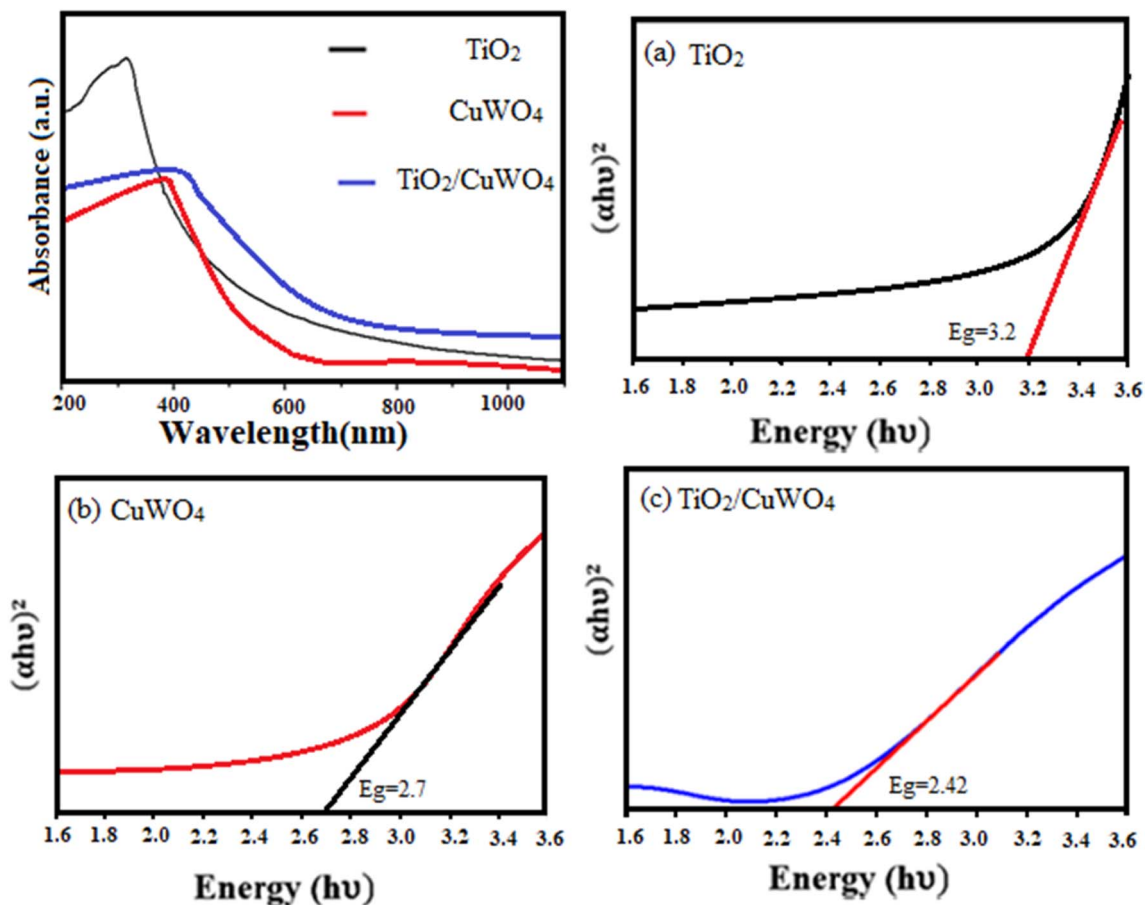


Fig. 6 UV-Vis spectrum of TiO₂/CuWO₄; the Tauc plots for TiO₂ (a), CuWO₄ (b), and TiO₂/CuWO₄ (c).

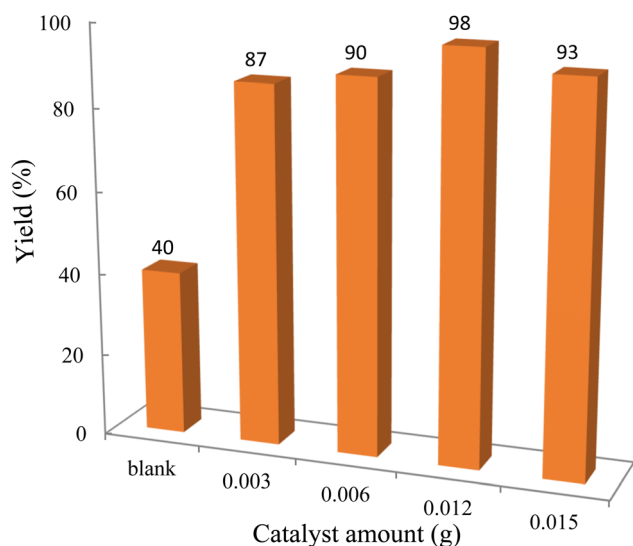


Fig. 7 Effect of photocatalyst on the yield of chromeno[4,3-*b*]chromene.

outperformed the other catalysts examined (Fig. 9). Additionally, Fig. 10 demonstrates how reaction temperature influences the process. Higher temperatures resulted in an increased reaction rate, attributed to greater molecular mobility and more

frequent collisions. Nonetheless, overly high temperatures can cause degradation and undesired side reactions. This study identified that both yield percentage and isolated yield are affected by the reaction temperature, with the best outcomes

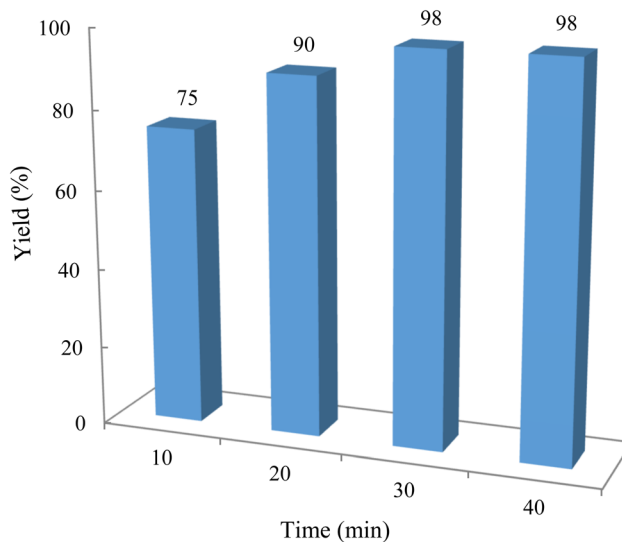


Fig. 8 Effect of reaction time.

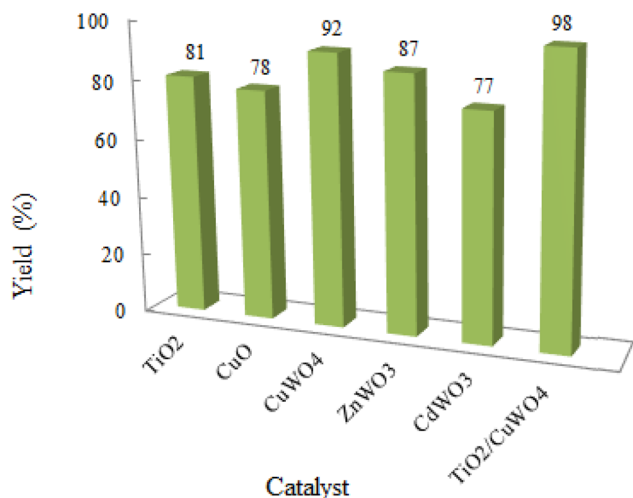


Fig. 9 Photocatalytic activity of some related photocatalysts in the condensation reaction.

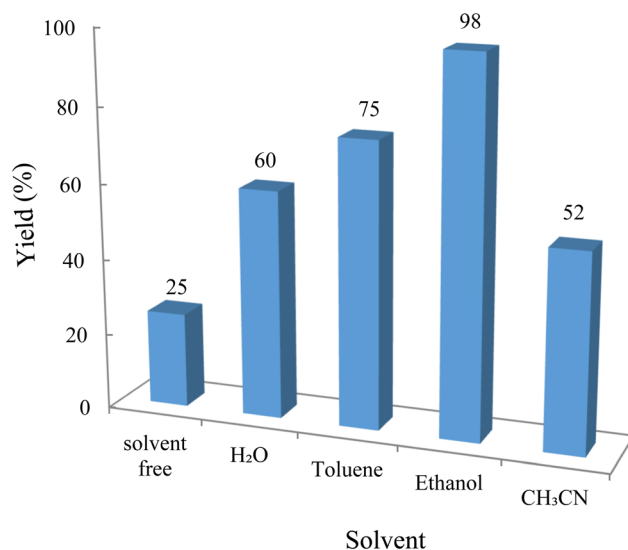


Fig. 11 Effect of different solvents.

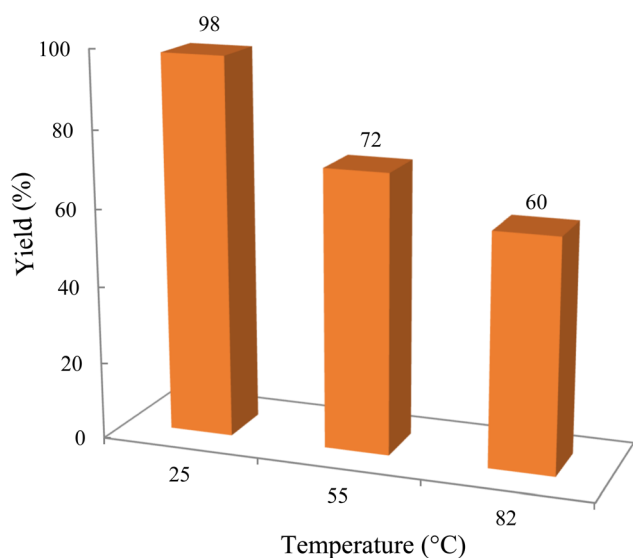


Fig. 10 Effects of reaction temperature.

observed at 25 °C. The effect of different solvents on the synthesis of chromeno[4,3-*b*]chromenes was also explored, revealing that ethanol was the most effective solvent under the optimal reaction conditions (Fig. 11).

3.2.2 Effect of different lights. When a photocatalyst like TiO₂/CuWO₄ is illuminated, it produces electron-hole pairs. The wavelength and energy of the light source are essential factors for maximizing photon absorption by the photocatalyst in optimal conditions. Moreover, the intensity of the light affects how quickly photons arrive at the photocatalyst surface. As light intensity rises, a greater number of photons can be absorbed, resulting in increased generation of electron-hole pairs. This study evaluated different light sources while maintaining consistent experimental conditions (Table S1†). The findings showed that a yield of 41% was obtained in darkness, while all other tested light sources generated yields over 90%.

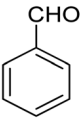
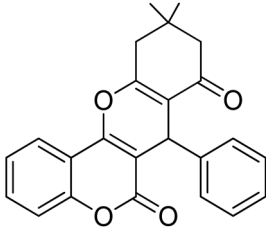
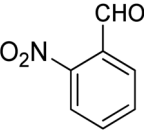
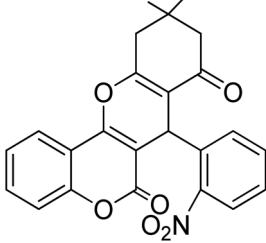
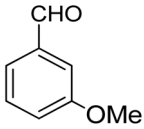
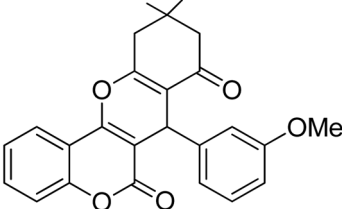
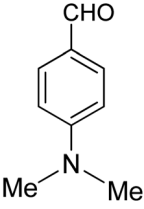
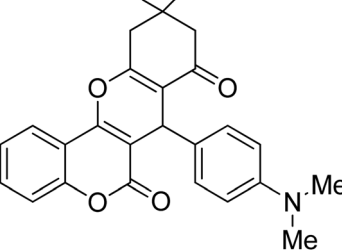
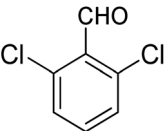
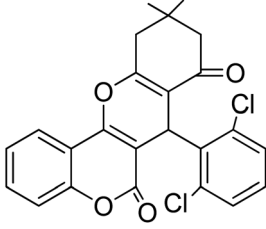
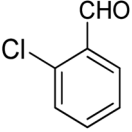
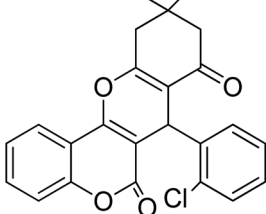
Ultimately, we chose the green laser light due to its environmentally friendly characteristics and economic advantages.

3.2.3 Preparation of substituted chromenes. To evaluate the applicability and consistency of the current protocol, a range of chromeno[4,3-*b*]chromenes was synthesized by altering the substituents on the phenyl ring of benzaldehyde (Table 1). The majority of the aromatic aldehydes tested, regardless of whether they featured electron-withdrawing or electron-donating groups, produced high yields under the optimal reaction conditions. This demonstrates the synthesis method versatility and efficacy across various substrates. The yields of the reaction can be significant. Electron-donating substituents such as -OCH₃ can increase electron density on the aromatic ring, thereby stabilizing the transition state and facilitating electrophilic attack, which results in improved yields. Conversely, substituents like -NO₂ draw electron density away from the aromatic ring, negatively impacting the reaction. The decrease in electron density renders the ring less nucleophilic and diminishes its reactivity with electrophiles. Consequently, with the presence of electron-withdrawing substituents, reactions generally result in lower conversions and less favorable yields, as the nucleophilic attack on the electrophilic reagent becomes more difficult.

The reaction involving dimedone (140 mg, 1 mmol), benzaldehyde (100 mg, 1 mmol), and 4-hydroxycoumarin (162 mg, 1 mmol) was carried out with TiO₂/CuWO₄ (0.012 g) in 4 mL of ethanol under the irradiation of a green laser at 25 °C for 30 minutes.

3.2.4 Hot filtration test. The hot filtration test is performed to confirm that the catalytic activity of TiO₂/CuWO₄ arises from the complete conjugated composite rather than from any leached components. To conduct this test, a standard condensation reaction was carried out with TiO₂/CuWO₄ (0.012 mg) for 15 minutes. Afterward, the catalyst was removed, resulting in a product yield of 55%. Following this, the reaction proceeded for an additional 15 minutes, resulting in a slightly better yield of 63%, based on the isolated chromene. Notably, extending the

Table 1 Substrate scope in the present condensation reaction

Entry	Aldehyde	Product	M.P. (°C)	Yield (%)
1			222–220	98
2			220–222	57
3			247–249	74
4			176–177	67
5			124–125	64
6			208–210	88

reaction time to one hour did not result in a meaningful increase in yield. This experiment clearly demonstrated that there was minimal leaching in the reaction medium.

3.2.5 Photocatalyst recycling and reuse. Assessing the recycling and reusability of the heterogeneous $\text{TiO}_2/\text{CuWO}_4$ photocatalyst is essential for understanding its practical utility.

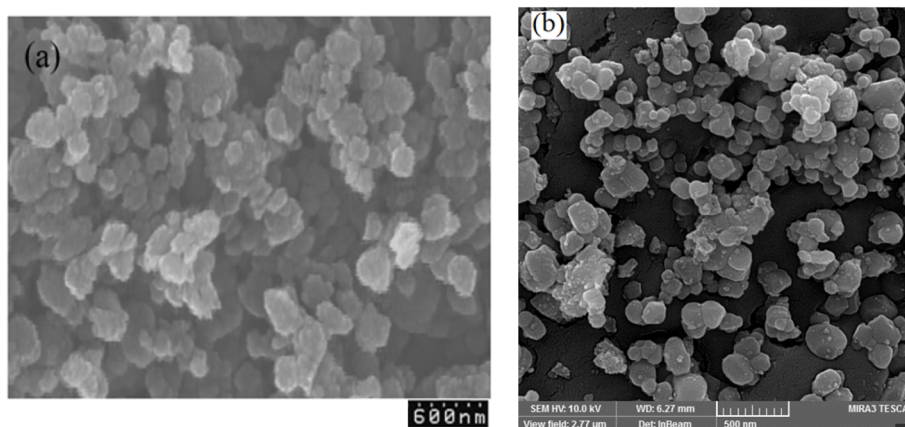


Fig. 12 SEM images of (a) reused and (b) fresh $\text{TiO}_2/\text{CuWO}_4$.

A fresh experiment was carried out to evaluate the photocatalyst performance over multiple uses in the target reaction. During this process, the photocatalyst was separated from the reaction mixture, rinsed with ethanol (EtOH), and air-dried prior to its reuse in later reactions. The findings of this study revealed that $\text{TiO}_2/\text{CuWO}_4$ displayed remarkable stability and reusability, as illustrated in Fig. S2.† This outcome emphasizes the photocatalyst suitability for sustainable applications, enabling it to retain its efficiency across several cycles without considerable degradation in performance. The spectral data obtained from the recycled catalyst were similar to that of the fresh catalyst, confirming that the structure of $\text{TiO}_2/\text{CuWO}_4$ was largely preserved throughout the reaction. To verify the integrity of TiO_2 and CuWO_4 in the reused photocatalyst, FT-IR analysis was conducted, comparing $\text{TiO}_2/\text{CuWO}_4$ with the fresh sample (Fig. S3a and b†). As expected, the characteristic stretching vibrations of TiO_2 and CuWO_4 were detected, indicating no significant destruction happened in the reused photocatalyst. Moreover, the SEM image of the recycled catalyst is compared with the fresh one, as confirmed no significant changes in the morphology of nanoparticles (Fig. 12).

4. Conclusion

Chromeno[4,3-*b*]chromenes represent a versatile and biologically active scaffold with significant implications for cardiovascular health. Their antioxidant and anti-inflammatory properties, along with potential vasodilatory effects, highlight their therapeutic promise. Therefore, it is crucial to create innovative, eco-friendly synthetic methods for these compounds. Heterojunction photocatalysts present numerous benefits compared to conventional homogeneous photocatalysts, such as improved charge separation, a wider spectrum of light absorption, greater stability and longevity, adjustable properties, and synergistic interactions. Titanium dioxide is recognized for its remarkable photocatalytic efficiency when compared to various other semiconductors, thanks to its extensive surface area and porous lattice structure. Nevertheless, its wide band gap restricts its absorption capability. To

overcome this challenge, $\text{TiO}_2/\text{CuWO}_4$ has been introduced to improve the performance of both TiO_2 and CuWO_4 . The synthesized photocatalyst underwent characterization utilizing a range of techniques, including FT-IR, XRD, UV-Vis, DRS, FE-SEM, TEM, EDS, and XPS. The $\text{TiO}_2/\text{CuWO}_4$ photocatalyst was subsequently utilized for the photocatalytic synthesis of substituted chromeno[4,3-*b*]chromenes and showed greater efficiency than the individual components. The study closely examined various factors, including the quantity of photocatalyst, reaction duration, temperature, choice of solvent, and the reusability of the photocatalyst. The results highlighted the importance of $\text{TiO}_2/\text{CuWO}_4$ heterojunction material in photocatalytic synthesis compared to other similar materials introduced in the field.

Data availability

The data that support the findings of this study are available from the authors.

Conflicts of interest

There are no conflicts to declare.

References

- 1 A. T. Benny, S. D. Arikatt, C. G. Vazhappilly, S. Kannadasan, R. Thomas, M. S. Leelabaiamma, E. K. Radhakrishnan and P. Shanmugam, Chromone, a privileged scaffold in drug discovery: developments in the synthesis and bioactivity, *Mini-Rev. Med. Chem.*, 2022, 22(7), 1030–1063.
- 2 B. Jadhaw, B. Gandhi, M. Jhansi, S. Misra and S. S. Kaki, Synthesis and Biological Evaluation of Novel Lipophilic Chromene Based 1,3,4-Oxadiazoles for Anti-cancer and Anti-inflammatory Activity, *Arabian J. Sci. Eng.*, 2024, 49(1), 221–230.
- 3 D. H. Dawood, A. M. Srour, D. O. Saleh, K. J. Huff, F. Greco and H. M. Osborn, New pyridine and chromene scaffolds as potent vasorelaxant and anticancer agents, *RSC Adv.*, 2021, 11(47), 29441–29452.

- 4 Y. Zhang, R. Jiang, L. Lei, Y. Yang and T. Hu, Drug delivery systems for oral disease applications, *J. Appl. Oral Sci.*, 2022, **30**, e20210349.
- 5 R. K. Kushwaha, K. Singh, P. Kumar and D. Chandra, Review on Chromen Derivatives and Their Pharmacological Activities, *Res. J. Pharm. Technol.*, 2019, **12**(11), 5566–5574.
- 6 V. Raj and J. Lee, 2H/4H-Chromenes-a versatile biologically attractive scaffold, *Front. Chem.*, 2020, **8**, 623.
- 7 E. M. Rojas, H. Zhang, S. E. Velu and H. Wu, Tetracyclic homoisoflavanoid (+)-brazilin: a natural product inhibits c-di-AMP-producing enzyme and *Streptococcus mutans* biofilms, *Microbiol. Spectrum*, 2024, **12**(5), e02418–e02423.
- 8 W. Y. Teoh, J. A. Scott and R. Amal, Progress in heterogeneous photocatalysis: from classical radical chemistry to engineering nanomaterials and solar reactors, *J. Phys. Chem. Lett.*, 2012, **3**(5), 629–639.
- 9 H. Yang, Short review on heterojunction photocatalysts: carrier transfer behavior and photocatalytic mechanisms, *Mater. Res. Bull.*, 2021, **142**, 111406.
- 10 G. Huang, Z. Jalili, R. Tayebee, Z. Shi, X. Zhang, L. Liu, L. Wang, D. Sun, X. Sun, L. Liu and W. Zhao, Zinc oxide-cadmium(II) sulfide heterostructure as a potential photocatalyst for preparing substituted chromenes and its anti-liver cancer activity, *Appl. Organomet. Chem.*, 2024, **38**(5), e7410.
- 11 B. Li, R. Tayebee, E. Esmaeili, M. S. Namaghi and B. Maleki, Selective photocatalytic oxidation of aromatic alcohols to aldehydes with air by magnetic $\text{WO}_3\text{ZnO}/\text{Fe}_3\text{O}_4$. In situ photochemical synthesis of 2-substituted benzimidazoles, *RSC Adv.*, 2020, **10**(67), 40725–40738.
- 12 S. Abbaspour, R. Zhou, F. M. Zonoz and R. Tayebee, Advanced $\text{CuO-Ag}_2\text{WO}_4\text{-Ni}$ nanophotocatalyst in the synthesis of some chromeno[4,3-b]chromenes as effective lung cancer drugs, *Inorg. Chem. Commun.*, 2024, **170**, 113284.
- 13 A. Balapure, J. Ray Dutta and R. Ganesan, Recent advances in semiconductor heterojunctions: a detailed review of the fundamentals of photocatalysis, charge transfer mechanism and materials, *RSC Appl. Interfaces*, 2024, **1**, 43–69.
- 14 M. Karami, A. Hasaninejad, H. Mahdavi, A. Iraj, S. Mojtavavi, M. A. Faramarzi and M. Mahdavi, One-pot multi-component synthesis of novel chromeno[4,3-b]pyrrol-3-yl derivatives as alpha-glucosidase inhibitors, *Mol. Diversity*, 2021, 1–3.
- 15 F. Kamali and F. Shirini, Melamine: an efficient promoter for some of the multi-component reactions, *Polycyclic Aromat. Compd.*, 2019, **41**, 73–94.
- 16 M. Aravind, M. Amalanathan and M. S. Mary, Synthesis of TiO_2 nanoparticles by chemical and green synthesis methods and their multifaceted properties, *SN Appl. Sci.*, 2021, **3**, 409.
- 17 B. Abdi, R. Tayebee, E. Rezaei-seresht, F. M. Zonoz and Z. Jalili, $\text{TiO}_2/\text{AgSbO}_3$ nanophotocatalyst with improved photocatalytic performance in the synthesis of some benzimidazole derivatives, *J. Mol. Struct.*, 2025, **1321**, 140037.
- 18 F. Ahmadi, M. Rahimi-Nasrabadi and M. Eghbali-Arani, The synthesize of CuWO_4 nano particles by a new morphological control method, characterization of its photocatalytic activity, *J. Mater. Sci.: Mater. Electron.*, 2017, **28**, 5244–5249.
- 19 P. Raizada, S. Sharma, A. Kumar, P. Singh, A. A. Khan and A. M. Asiri, Performance improvement strategies of CuWO_4 photocatalyst for hydrogen generation and pollutant degradation, *J. Environ. Chem. Eng.*, 2020, **8**(5), 104230.
- 20 Z. Jalili, R. Tayebee and F. M. Zonoz, Eco-friendly synthesis of chromeno[4,3-b]chromenes with a new photosensitized $\text{WO}_3/\text{ZnO}@\text{NH}_2\text{-EY}$ nanocatalyst, *RSC Adv.*, 2021, **11**(29), 18026–18039.
- 21 M. Jarrahi, B. Maleki and R. Tayebee, Magnetic nanoparticle-supported eosin Y salt [SB-DABCO@eosin] as an efficient heterogeneous photocatalyst for the multi-component synthesis of chromeno[4,3-b]chromene in the presence of visible light, *RSC Adv.*, 2022, **12**(45), 28886–28901.
- 22 Z. Barzgar, S. Z. Askari and A. Ghazizadeh, Fabrication of nanostructured CuWO_4 for photocatalytic degradation of organic pollutants in aqueous solution, *J. Mater. Sci.: Mater. Electron.*, 2017, **28**, 3293–3298.
- 23 S. Zhou, Y. Wang, G. Zhao, C. Li, L. Liu and F. Jiao, Enhanced visible light photocatalytic degradation of rhodamine B by Z-scheme $\text{CuWO}_4/\text{gC}_3\text{N}_4$ heterojunction, *J. Mater. Sci.: Mater. Electron.*, 2021, **32**, 2731–2743.
- 24 J. L. Gole, J. D. Stout, C. Burda, Y. Lou and X. Chen, Highly efficient formation of visible light tunable $\text{TiO}_2\text{-xN}_x$ photocatalysts and their transformation at the nanoscale, *J. Phys. Chem. B*, 2004, **108**(4), 1230–1240.
- 25 X. Zhu, G. Wen, H. Liu, S. Han, S. Chen, Q. Kong and W. Feng, One-step hydrothermal synthesis and characterization of Cu-doped TiO_2 nanoparticles/nanobucks/nanorods with enhanced photocatalytic performance under simulated solar light, *J. Mater. Sci.: Mater. Electron.*, 2019, **30**, 13826–13834.